Stressing-Out DNA? The Contribution of Serine−Phosphodiester Interactions in Catalysis by Uracil DNA Glycosylase†

R. Marshall Werner, Yu Lin Jiang, Russell G. Gordley, G. Jayashree Jagadeesh, Jane E. Ladner, Gaoyi Xiao, Maria Tordova, Gary L. Gilliland, and James T. Stivers*

Center for Advanced Research in Biotechnology, University of Maryland Biotechnology Institute and National Institute for Standards and Technology, 9600 Gudelsky Drive, Rockville, Maryland 20850

Received July 5, 2000; Revised Manuscript Received August 11, 2000

ABSTRACT: The DNA repair enzyme uracil DNA glycosylase (UDG) pinches the phosphodiester backbone of damaged DNA using the hydroxyl side chains of a conserved trio of serine residues, resulting in flipping of the deoxyuridine from the DNA helix into the enzyme active site. We have investigated the energetic role of these serine−phosphodiester interactions using the complementary approaches of crystallography, directed mutagenesis, and stereospecific phosphorothioate substitutions. A new crystal structure of UDG bound to 5′-HO-dUAAp-3′ (which lacks the 5′ phosphodiester group that interacts with the Ser88 pinching finger) shows that the glycosidic bond of dU has been cleaved, and that the enzyme has undergone the same specific clamping motion that brings key active site groups into position as previously observed in the structures of human UDG bound to large duplex DNA substrates. From this structure, it may be concluded that glycosidic bond cleavage and the induced fit conformational change in UDG can occur without the 5′ pinching interaction. The S88A, S189A, and S192G "pinching" mutations exhibit 360-, 80-, and 21-fold damaging effects on k_{cat}/K_m, respectively, while the S88A/S189A double mutant exhibits an 8200-fold damaging effect. A free energy analysis of the combined effects of nonbridging phosphorothioate substitution and mutation at these positions reveals the presence of a modest amount of strain energy between the compressed 5′ and 3′ phosphodiester groups flanking the bound uridine. Overall, these results indicate a role for these serine−phosphodiester interactions in uracil flipping and preorganization of the sugar ring into a reactive conformation. However, in contrast to a recent proposal [Parikh, S. S., et al. (2000) *Proc Natl. Acad. Sci*. *94*, 5083], there is no evidence that conformational strain of the glycosidic bond induced by serine pinching plays a major role in the 10^{12}-fold rate enhancement brought about by UDG.

Enzymes that remove damaged bases from DNA have evolved under the highest evolutionary pressure to form highly specific interactions with damaged sites in DNA without any preference for the sequence context in which the damaged base is located. The penalty for catalytic sloppiness is the removal of normal bases and the excessive introduction of abasic sites in DNA, which are highly cytotoxic (*1*). Accordingly, the binding interactions that lead to such high specificity and catalytic power must be found in the unique features of the damaged site, or in the repetitive features of the DNA backbone such as the phosphodiester linkage.

A premier example of such highly evolved specificity and catalytic power is found in the DNA repair enzyme uracil DNA glycosylase (UDG), which hydrolytically removes uracil from both single-stranded and duplex DNA (*2*). Uracil may arise in DNA through two independent pathways: the spontaneous deamination of cytosine residues and the misincorporation of dUTP during DNA replication. The intervention of UDG in the first pathway is beneficial because it prevents CG → AT transition mutations. The importance of the latter pathway depends critically on the dUTP/TTP pool in the cell. Under certain conditions, such as folate deficiency, or upon treatment with the cancer chemotherapeutic agent 5-fluorouracil, the extent of conversion of dUMP to TMP by thymidylate synthetase is diminished and massive amounts of uracil can be accumulated in human cellular DNA (*3*). When two closely spaced uracils are located on opposite strands of the DNA, the sequential action of UDG and an apyrimidinic endonuclease produces double-strand breaks, which can lead to apoptosis or cancer. Accordingly, DNA repair has been aptly termed a double-edged sword (*4*).

We have been systematically investigating the interactions of UDG with substrate and transition-state analogues to better understand the nature of the forces that lead to specificity and highly efficient catalysis. As suggested by both crystallographic and biophysical studies (*5*−*7*), the earliest step in damaged site recognition by UDG is compression of the DNA phosphodiester backbone, leading to torsional stress in the DNA duplex (Figure 1). Stress is likely introduced by the pinching action of three conserved serine residues of UDG which hydrogen bond with three adjacent phosphodiester groups located on a single strand of the DNA (Ser88, Ser189, and Ser192 of *e*UDG).[1] Upon encounter of the uracil site, the stress is presumably relieved by flipping the entire

† This work was supported by NIH Grant RO1 GM56834 (J.T.S.) and the National Institute for Standards and Technology.

* To whom correspondence should be addressed. Phone: (301) 738-6264. Fax: (301) 738-6255. E-mail: stivers@carb.nist.gov.

10.1021/bi001532v CCC: $19.00
Published on Web 09/19/2000

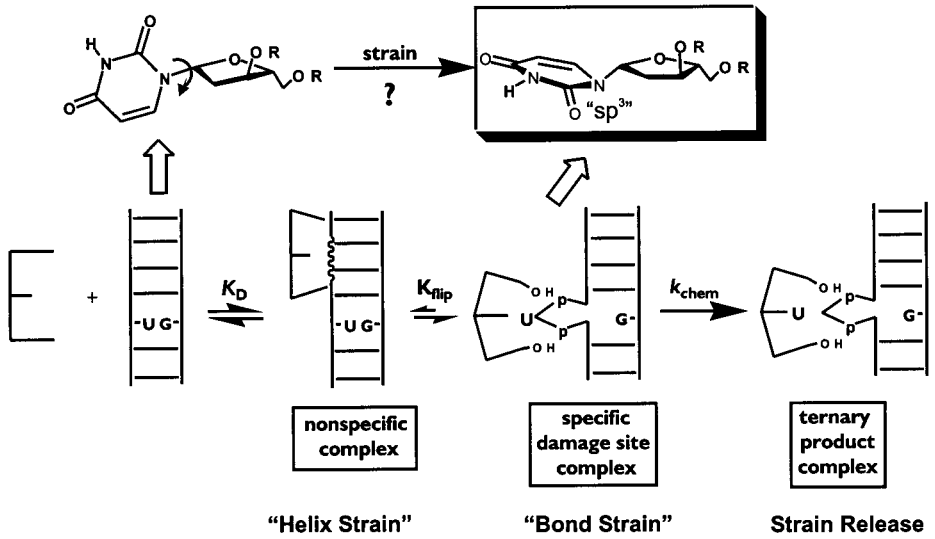

FIGURE 1: Schematic mechanism for uracil site location, base flipping, and catalysis by UDG invoking the two roles for strain as proposed by Tainer and colleagues (*6*, *7*). In the first role, the side chain hydroxyls of three conserved serine residues (S88, S189, and S192) compress the phosphodiester backbone of DNA when the enzyme interacts nonspecifically with DNA, thereby exerting a torsional stress on the duplex ("Helix Strain"). The stress is relieved when the uracil site is encountered by flipping the uracil from the DNA base stack (only two serines are depicted for clarity). In a second role for strain, it has been suggested that the enzyme significantly bends the glycosidic bond in deoxyuridine to a tetrahedral geometry ("Bond Strain"), thereby allowing favorable orbital overlap and electron flow between O4′ and O2 of the uracil in a dissociative transition state (see also Scheme 1 in the Discussion) (*6*). This orbital steering mechanism was proposed to require the 5′ and 3′ serine phosphodiester interactions, and the rigid walls imposed by the active site aromatic groups Phe77 and Tyr66 (not shown) (*6*). According to this model, strain is relieved upon glycosidic bond cleavage, leading to tight binding of the abasic product which protects the site until the repair process can be completed. The hypothetical structure that is shown for the flipped-out deoxyuridine is based on the observed tetrahedral arrangement of the glycosidic C1 atom in the crystal structure of UDG bound to DNA-containing deoxypseudouridine (see also Scheme 1 in the Discussion) (*6*).

deoxyuridine nucleotide from the helical stack into the highly specific active site pocket of the enzyme. Such an induced strain mechanism for base flipping by UDG is suggested by the observation (i) that binding of undamaged B-DNA would produce steric clashes with the serine loops of the enzyme without the DNA first being kinked (*7*) and (ii) that the earliest kinetic step in damaged site recognition is weak nonspecific DNA binding (*5*). Recent model studies have provided plausible support for the involvement of strain in base flipping by showing that duplex DNA itself can relax by extruding a base from the helix when strain is introduced by an artificial cross-link in the minor groove (*8*). From this model system, the strain energy required to extrude a cytosine base from a G·C base pair was estimated to be only 12 kJ/mol, indicating that the binding energies of enzymes with their DNA substrates are easily sufficient to produce similar contortions in DNA structure.

Tainer and colleagues, on the basis of their crystal structure of *h*UDG bound to DNA containing the stable C-glycoside substrate analogue deoxypseudouridine, have proposed that strain induced by serine pinching is also used to dramatically lower the activation barrier for glycosidic bond cleavage (*6*). This proposal was based upon the unexpected observation that the normally trigonal planar C1 position of deoxypseudouridine (corresponding to N1 in deoxyuridine) was bent toward a tetrahedral geometry (Figure 1). It was argued that such a conformation, if effected in the natural substrate, would lead to enhanced electron orbital overlap between the glycosidic bond and the π-systems of the uracil ring. The putative catalytic benefits of stereoelectronic effects have been proposed and disputed for more than 25 years for a number of glycosidic bond cleavage reactions (*9*).

What is the contribution of serine pinching in base flipping and in reducing the activation barrier for glycosidic bond cleavage? In this study, we begin to address this question by using the complementary approaches of directed mutagenesis and phosphorothioate substitutions, and we report the first crystal structure of UDG bound to single-stranded dU-containing DNA. Disruption of these individual serine pinching interactions, by either stereospecific phosphorothioate substitution or deletion mutagenesis, leads to 10−400-fold damaging effects on DNA binding and transition-state stabilization. The crystal structure with the bound substrate 5′-HO-dUAAp-3′ [which lacks the 5′ phosphodiester group that interacts with the conserved Ser88 pinching residue (Figure 1)] shows that the enzyme has cleaved the glycosidic bond, and undergone the same induced fit conformational change that has been observed previously for large duplex DNA substrates (*6*, *7*). Thus, the induced fit conformational change in UDG, and cleavage of the glycosidic bond, can proceed in the absence of this serine−phosphodiester interaction. The results suggest that if serine pinching plays a role in conformational strain in the ground state (*6*), then this strain contributes no more than 22 kJ/mol toward the reduction in the activation barrier of the reaction ES $\rightarrow$ ES‡. This upper limit contribution from strain is similar to that obtained from chemical catalysis (*10*−*12*), and does not in itself account for a majority of the catalytic power of UDG as recently proposed (*6*).

[1] Abbreviations: *e*UDG, *Escherichia coli* uracil DNA glycosylase; *h*UDG, human uracil DNA glycosylase; **P**, 2-aminopurine; MALDI, matrix-assisted laser desorption ionization mass spectrometry.

EXPERIMENTAL PROCEDURES[2]

Oligonucleotide Synthesis. The phosphodiester and racemic phosphorothioate (Ps) substrates of the sequence ApUp**P**pA were synthesized using standard phosphoramidite chemistry with an Applied Biosystems 390 synthesizer. The nucleoside phosphoramidites and the sulfurizing reagent were purchased from Applied Biosystems or Glen Research (Sterling, VA). After synthesis and deprotection, the phosphodiester oligonucleotides were purified by anion exchange HPLC and desalted by C-18 reversed phase HPLC (Phenomenex Aqua column). The racemic Ps substrates were first purified by anion exchange HPLC, and then the R_p and S_p diastereomers were resolved by C-18 reversed phase chromatography with isocratic elution using 10% acetonitrile containing 0.1 M TEAA (pH 7.5). The size, purity, and nucleotide composition of the DNA were assessed by analytical reversed phase HPLC and MALDI mass spectrometry. The configuration and stereochemical purity of the Ps oligonucleotides were determined by RP-HPLC of the free nucleosides after digestion with snake venom phosphodiesterase, nuclease P1, and alkaline phosphatase (*13*). The (R_p)-Ps and (S_p)-Ps oligonucleotides used in this work were of more than 99% stereochemically pure. The concentrations were determined by UV absorption measurements at 260 nm, using the pairwise extinction coefficients for the constituent nucleotides (*14*).

Purification of UDG. UDG from *Escherichia coli* strain B was purified to >99% homogeneity using a T7 polymerase-based overexpression system as described previously (*10*, *15*). The concentration of the enzyme was determined using an extinction coefficient of 38.511 mM^{-1} cm^{-1} (*10*). The S88A, S189A, S192G, and S88A/S189A mutants were generated using the *Quik-Change* double-stranded mutagenesis kit from Stratagene (La Jolla, CA). The mutations were confirmed by sequencing both strands of the DNA, and the six-His-tagged mutant proteins were purified using nickel chelate chromatography as previously described (*10*, *15*).

Crystallography. The complex between Y19H *e*UDG and dUAAp was crystallized at 20 °C by vapor diffusion in hanging drops of equal volumes of complex solution and well solution [0.1 M HEPES (pH 7.5), 2% PEG 400, and 2.0 M ammonium sulfate]. The Y19H mutant has been shown in previous biochemical and crystallographic studies to be identical to the wild-type enzyme in activity and structure (*15*). The complex was prepared by mixing the protein stock solution (14.9 mg/mL, or 0.6 mM) with the dUAAp stock solution (2.4 mM) in a volume ratio of 1:3.8. The crystals grew to full size over the course of 6 weeks. Crystals were soaked in the cryoprotectant glycerol, and diffraction data were collected at 100 K using a Bruker electronic area detector and rotating anode X-ray generator. All data were indexed and processed using the XENGEN suite of programs (*16*). The structure was determined using the molecular replacement method with the free wild-type structure as a probe. Structural refinement was performed with the programs X-PLOR (*17*) and SHELX-97 (*18*). The coordinates have been deposited in the Protein Data Bank.[3]

Steady-State Kinetic Measurements and Cleavage Assays. The steady-state kinetics of uracil glycosidic bond cleavage were determined at 25 °C in TMN buffer [10 mM Tris-HCl (pH 8.0), 2.5 mM $MgCl_2$, and 25 mM NaCl] using the 2-aminopurine continuous fluorescence assay as previously described (*10*, *19*). The steady-state kinetic parameters k_{cat} and k_{cat}/K_m were obtained from plots of the observed rate constants (k_{obsd}) against substrate concentration ($[S]_{tot}$) using a standard hyperbolic kinetic expression and the program *Grafit 4* (*20*) according to eqs 1 and 2:

$$k_{obsd} = (1/\Delta a)(\Delta F/\Delta t)(1/[UDG]_{tot}) \quad (1)$$

$$k_{obsd} = k_{cat}/(K_m + [S]) \quad (2)$$

In eq 2, $\Delta F/\Delta t$ is the initial rate in fluorescence units per second, ΔF_{tot} is the total fluorescence increase for 100% conversion of a given substrate concentration ($[S]_{tot}$) to product, $\Delta a = \Delta F_{tot}/[S]_{tot}$, and $[UDG]_{tot}$ is the total UDG concentration. The values for Δa were determined either by letting the reaction go to completion or by adding 10−20 nM wild-type UDG to rapidly bring the reaction to its end point after completing the initial rate measurements. For the time-base scans, an excitation wavelength of 310 or 320 nm was used, and the emission was observed at 370 nm.

RESULTS

General Approach. The goal of this study is to determine the energetic role of serine pinching in damage site recognition and catalysis by UDG. We have addressed this question using two complementary approaches: directed mutagenesis and stereospecific phosphorothioate (Ps) substitution. As will be shown below, the value of using both approaches is that direct and indirect interactions of active site groups with individual phosphodiester oxygens can be ascertained and quantified. UDG is ideal for such a study because its substrate specificity extends to small single-stranded dU-containing DNA substrates (*21*). Indeed, we have previously shown that the small 5mer substrate AU**P**AA has the same single-turnover rate of glycosidic bond cleavage as observed with larger 19mer duplex substrates ($k_{max} \sim 150\ s^{-1}$) (*10*). In this work, we employ a similar 4mer substrate, AU**P**A (Figure 2), that represents the smallest substrate for UDG that still retains full catalytic activity ($k_{max} = 110\ s^{-1}$) (*22*). This small oligonucleotide construct allows facile incorporation of nonbridging phosphorothioate groups at each phosphodiester linkage and permits baseline resolution of the R_p and S_p diastereomers using reversed phase HPLC (not shown). This detailed work using single-stranded DNA provides the foundation for comparative studies of the role of serine pinching in base flipping in duplex DNA (*22*).

Rigorous interpretation of mutational effects and thio effects requires consideration of the rate-limiting steps of the steady-state reaction. We have previously shown that product release is severely rate-limiting for k_{cat} measurements for wild-type UDG, but not for slow mutant enzymes or slow substrates (*10*). Accordingly, measurements of the damaging

[2] Certain commercial equipment, instruments, and materials are identified in this paper to specify the experimental procedure. Such identification does not imply recommendation or endorsement by the National Institute of Standards and Technology, nor does it imply that the material or equipment identified is necessarily the best available for the purpose.

[3] Research Collaboratory for Structural Bioinformatics Protein Data Bank (entry 1FLZ).

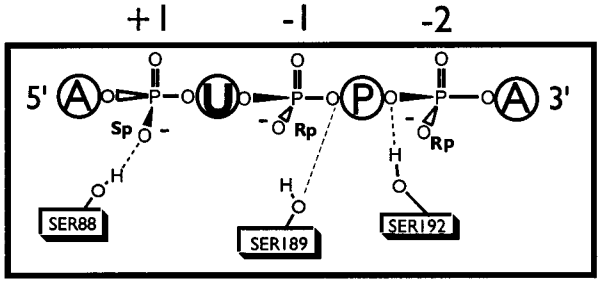

FIGURE 2: Structure of the single-stranded DNA substrate used here (**P** is 2-aminopurine). The phosphodiester interactions with the three serine side chains are based on the crystal structure and the combined thio effect and mutational effect studies reported in this study.

effects of mutations or sulfur substitution are nearly always influenced by changes in the rate-limiting step. To avoid this problem in the interpretation of the kinetic data presented here, we only compare the k_{cat}/K_m values quantitatively, because this constant is unaffected by the product release step (k_3), and only reports on the kinetic steps between substrate binding (k_1) and the first irreversible step of glycosidic bond cleavage (k_2), as shown in eqs 3−5.

$$E + S \underset{k_{-1}}{\overset{k_1}{\rightleftharpoons}} E{\cdot}S \xrightarrow{k_2} E{\cdot}AB{\cdot}U \xrightarrow{k_3} E + AB + U \quad (3)$$

$$k_{cat} = \frac{k_2 k_3}{k_2 + k_3} \quad (4)$$

$$k_{cat}/K_m = \frac{k_1 k_2}{k_{-1} + k_2} \quad (5)$$

In these equations, E is the enzyme, S is the substrate, AB is the abasic DNA product, and U is the uracil product. The steady-state kinetic parameters for the phosphodiester and phosphorothioate substrates as determined for the wild-type and mutated UDG enzymes are reported in Table 1.

Directed Mutagenesis of Conserved Serines. Representative initial rate data for uracil cleavage from the substrate AU**P**A by wild-type UDG and S88A mutant are shown in Figure 3A (note the 400-fold greater S88A concentration compared to that of the wild-type enzyme). The measured initial rates displayed a hyperbolic substrate concentration dependence (Figure 3B), from which the steady-state kinetic parameters k_{cat}, k_{cat}/K_m, and K_m were determined by nonlinear least-squares fitting to eq 2. The mutational effects (MEs) on k_{cat}/K_m for the S88A, S189A, and S192G mutants and the double mutant S88A/S189A are reported in Table 1 [ME $= (k_{cat}/K_m)^{wt}/(k_{cat}/K_m)^{mut}$]. The largest single mutational effect is seen for S88A (360-fold), and this residue is suggested to interact with the +1 phosphodiester of the substrate $Ap^{+1}Up^{-1}\mathbf{P}p^{-2}A$ as shown in the crystal structures discussed below. The damaging effects of removing Ser189 and Ser192 (which interact with the −1 and −2 phosphodiesters; see below and Figure 2) are about 4- and 17-fold lower than that of S88A, respectively. Therefore, individually, these three serine-pinching residues are important, but not required for catalysis. The double mutant S88A/S189A exhibits a significant 8200-fold mutational effect on k_{cat}/K_m, but even this doubly crippled enzyme is capable of catalyzing glycosidic bond cleavage about 10^8-fold faster than the spontaneous reaction in the absence of enzyme. This 8200-fold effect is 3.5-fold lower than the product of the two single-mutation effects on k_{cat}/K_m (360 × 80 = 28800-fold), indicating a small energetic coupling between S88 and S189 in the transition state (vida infra).

In addition to the damaging effects on k_{cat}/K_m, removal of these serine hydroxyl groups weakens substrate binding by about 10−60-fold (see the K_m values in Table 1). Interestingly, the S88A/S189A double mutant has a K_m value that is intermediate between that of either single mutant, indicating that the S189A mutation suppresses the S88A mutational effect on substrate binding. This differs from the effects of the double mutation on k_{cat}/K_m (see above), indicating

Table 1: Steady-State Kinetic Parameters, Mutational Effects (MEs), and Thio Effects (TEs)[a]

			+1 A$_{ps}$UPA (TE)			−1 AU$_{ps}$PA (TE)			−2 AUP$_{ps}$A (TE)		
	AUPA	AUPA (ME)	R_p	S_p	R_p/S_p	R_p	S_p	R_p/S_p	R_p	S_p	R_p/S_p
					Wild-Type UDG						
k_{cat} (s^{-1})	24.9 ± 2.3		1.5	22	0.07	7.4	1.2	6.2	1.4	1.4	1
K_m (μM)	2.9 ± 0.6		0.16	0.3	0.53	2.8	0.4	7	0.04	3.3	0.012
k_{cat}/K_m ($\mu M^{-1}\,s^{-1}$)	8.6 ± 2		9.2	67	0.14	2.7	3.2	0.8	33	0.4	82
					S88A						
k_{cat} (s^{-1})	4.5 ± 0.7	5.5	7.9	22	0.4	35	59	0.6			
K_m (μM)	186 ± 45	0.016	0.4	9	0.04	2.5	2.7	0.9			
k_{cat}/K_m ($\mu M^{-1}\,s^{-1}$)	0.02 ± 0.007	360	18.5	2.4	7.7	14	22	0.6			
					S189A						
k_{cat} (s^{-1})	2.6 ± 0.2	9.5	3.9	7.2	0.5	8.6	5	1.7			
K_m (μM)	24.5 ± 3.8	0.11	0.6	1.7	0.4	4.2	1.8	2.3			
k_{cat}/K_m ($\mu M^{-1}\,s^{-1}$)	0.11 ± 0.02	80	7.2	4.2	1.7	2.1	2.8	0.7			
					S192G						
k_{cat} (s^{-1})	16.7 ± 2.5	1.5								1	
K_m (μM)	41 ± 9.8	0.07								2.6	
k_{cat}/K_m ($\mu M^{-1}\,s^{-1}$)	0.4 ± 0.11	21							18[b]	0.4	45
					S88A/S189A						
k_{cat} (s^{-1})	0.051 ± 0.003	490									
K_m (μM)	49 ± 7	0.06									
k_{cat}/K_m ($\mu M^{-1}\,s^{-1}$)	0.001 ± 0.0002	8200									

[a] Kinetic parameters were determined at 25 °C in TMN buffer. The ME is defined as k^{wt}/k^{mut}, and the TE is defined as k^{ox}/k^{Ps}. The errors in the thio effects and mutational effects were ≤35%. [b] Only k_{cat}/K_m was determined due to the high K_m values for this reaction.

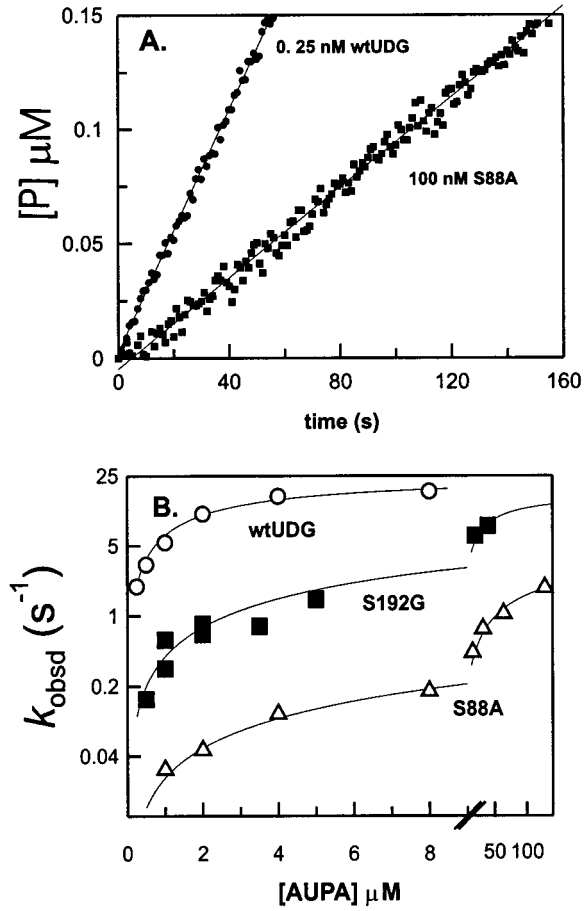

FIGURE 3: Representative steady-state kinetic data. (A) Time-dependent changes in 2-aminopurine (**P**) fluorescence accompanying cleavage of the glycosidic bond of the adjacent dU residue in the substrate ApUp**P**pA by wild-type and S88A UDG. (B) Substrate concentration dependence of the observed steady-state rates of cleavage for wild-type, S192G, and S88A UDG. The full kinetic results are reported in Table 1.

different energetic couplings between these groups in the ground state and transition state.

For the reasons noted above and in a previous study (*10*), mutational effects on k_{cat} are much smaller than k_{cat}/K_m, and do not reflect the full effect of the mutation on the chemical step of the reaction. However, an estimate of the true effect of a mutation on the kinetic barrier for conversion of the Michaelis complex to the transition state can be made by comparing the k_{cat} values for the mutant enzymes with the single-turnover k_{max} value of the wild-type enzyme [k_{max}(AUAA) = 110 s^{-1}]. Since k_{max} is about 5-fold faster than k_{cat} for the wild-type enzyme, then the true mutational effects on the conversion of ES to ES‡ should be about 5-fold greater than the measured mutational effects on k_{cat} reported in Table 1. When this approximate correction was made, the mutational effects on the chemical step were 28-, 48-, 8-, and 2500-fold for the S88A, S189A, S192G, and S88A/S189A mutants, respectively.

Stereospecific Phosphorothioate (Ps) Effects. Chiral phosphorothioates can serve as sensitive probes of enzyme contacts with phosphodiester groups (*23*−*25*) (*26*). Thio effects (TE, defined as k^{ox}/k^{Ps}) arise from a variety of factors that stem from the longer P−S^- bond length, and its lower electronegativity and altered charge distribution as compared to those of the P−O bond (*27*). In general, a nonbridging sulfur will give rise to weaker binding interactions with an enzymatic group because of the weaker hydrogen bond acceptor potential of sulfur compared to that of oxygen, leading to a thio effect that is greater than 1.

Combined thio effect and mutation studies have been useful in determining which enzyme side chains interact with a given phosphodiester oxygen, and in determining the energetic importance of such interactions (*24*, *26*). In the simplest case, if an enzymatic group interacts directly with a nonbridging oxygen, then the thio effect should be smaller for a mutant enzyme that lacks this group because the favorable interaction was already lost by deletion of the side chain by mutagenesis. In contrast, if there is little change in the thio effect for a mutant enzyme, then this provides evidence that the wild-type side chain does not interact with the nonbridging oxygen (see below). Although mutation of a residue that interacts directly with the nonbridging atom would be expected to produce the largest change in the thio effect (*26*), significant changes may also occur if the mutated group alters the structure of the complex, thereby indirectly changing the interaction of the nonbridging oxygen with the enzyme (*25*). Thus, the interpretation of an altered thio effect upon mutagenesis is best done in conjunction with structural information, such as that provided by the crystal structures described below.

The stereospecific thio effects on k_{cat}/K_m for wild-type UDG and each of the serine mutants are reported in Table 1. For the +1 (R_p)-Ps substitution, similar thio effects in the range of 7−18 are observed for the wild type, S88A, and S189A, indicating that the Ser88 and Ser189 hydroxyls do not strongly interact, either directly or indirectly, with the +1 pro-R_p oxygen. (This conclusion is supported by the crystal structure described below.) In contrast, the +1 S_p thio effect is 67 for the wild-type enzyme, and decreases by 16- and 28-fold upon removal of the Ser88 and Ser189 side chains, indicating that Ser88 and Ser189 interact with the +1 pro-*S*p oxygen. As reported in Table 1, there is a strong stereoselectivity to the thio effect at the +1 position, with the S_p isomer showing the largest effect with wild-type UDG, and the R_p isomer showing the largest effect with each of the mutants (the stereoselectivity is defined as TE^{R_p}/TE^{S_p} in Table 1).

For the −1 position, the changes in the thio effects upon mutation are strikingly different than those noted above for the +1 position. In this case, the thio effects for the S189A mutant and the wild-type enzyme are very similar (2−3-fold for both nonbridging positions), but the S88A mutation increases the −1 R_p and S_p thio effects by 14- and 22-fold (Table 1). This result indicates that Ser88 is energetically coupled to both of the −1 nonbridging oxygens. For the wild-type enzyme, the largest thio effect is seen for the R_p isomer, but for either mutant, there appears to be no strong stereoselectivity to the thio effect at the −1 position (Table 1).

At the −2 position, there is a large normal thio effect on k_{cat}/K_m for the R_p isomer using the wild-type enzyme (TE = 33), and a modest inverse thio effect of 2.5 for the S_p isomer (i.e., k_{cat}/K_m is larger upon −2 S_p sulfur substitution, Table 1). Thus, the largest stereoselective thio effect of the three sites is observed at this position (TE^{R_p}/TE^{S_p} = 82). The S192G mutant, which is located within hydrogen bonding distance of the −2 phosphodiester in the crystal structure (see below), exhibits thio effects similar to that of the wild-

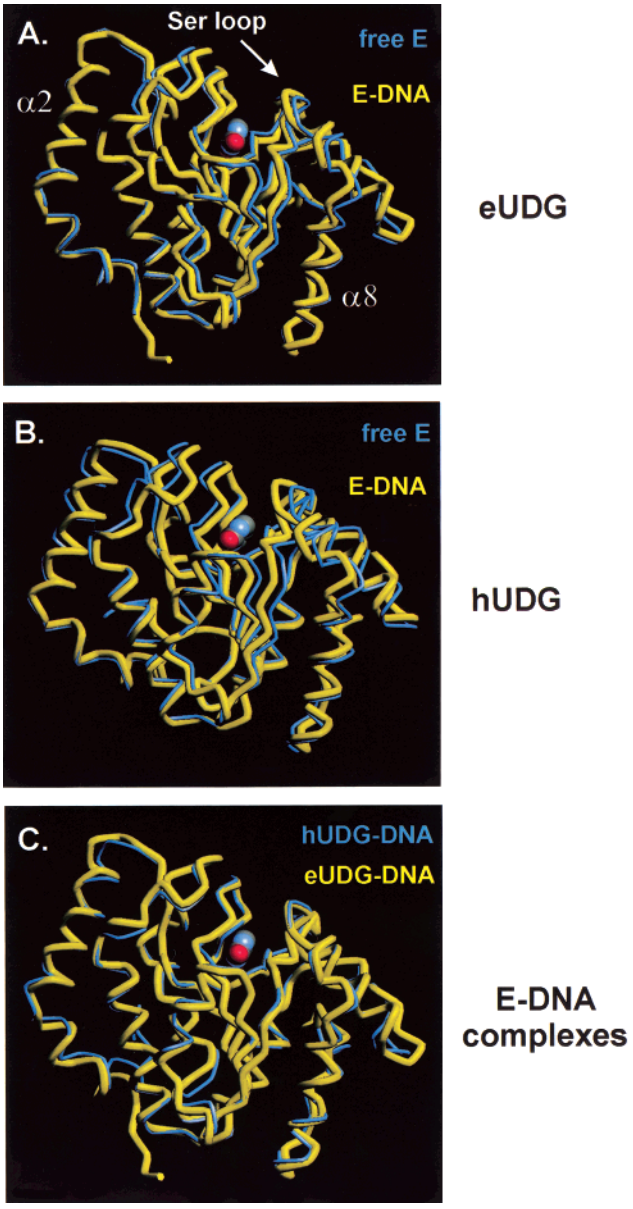

FIGURE 4: Comparison of the induced fit conformational changes in *h*UDG and *e*UDG upon productive binding of duplex and single-stranded DNA. (A) Alignment of the crystal structures of free *e*UDG (blue, Protein Data Bank entry 1eug) and its complex with the products of dUAAp (yellow). The AB trinucleotide is disordered in the product complex, and only the uracil base is shown. A clamping motion of active site loops is observed, and a slight displacement of helix 8. This same movement of the active site loops and helix 8 is seen with hUDG (see panel B), although to a slightly lesser extent because the active site of free eUDG more closely resembles the DNA-bound state than free *h*UDG (*15*). (B) Alignment of the crystal structures of free *h*UDG (blue) and its complex with duplex 11mer AB DNA and uracil (yellow, Protein Data Bank entry 1ssp). The same movements noted above for eUDG are observed, and an additional movement of helix 2 is seen. For clarity, the DNA has been omitted from this alignment. (C) Alignment of the crystal structures of the product complexes of *h*UDG (blue) and *e*UDG (yellow). The conformations of the DNA-bound enzymes are essentially identical, despite the large differences in the nature of the substrates.

type enzyme at the −2 position, suggesting that the side chain of Ser192 does not interact with either nonbridging oxygen at this site.

In summary, significant and stereospecific thio effects are observed at the +1, −1, and −2 positions, indicating strong interactions of the enzyme with these phosphodiester groups. In addition, Ser88 and Ser189 are energetically coupled to the +1 and −1 nonbridging oxygens, suggesting that these functional groups communicate, either directly or indirectly. These observations are further interpreted after presentation of the structural studies reported below.

Table 2: Data and Refinement Statistics for the *e*UDG Complex with dUAAp

diffraction data	
space group	$P4_32_12$
cell parameters (*a*, *b*, *c*) (Å)	78.2, 78.2, 80.8
content of the asymmetric unit	monomer
V_m (Å^3/Da)	2.4
no. of measured intensities	79612
no. of unique reflections	11146
R_{merge}	0.14
R_{merge}	0.26
completeness (36.0−2.3 Å) (%)	96
refinement using the data range 20.0−2.3 Å	
R-factor	0.27
no. of residues in the final coordinate file	228
no. of water molecules	124
rms deviations	
bond lengths (Å)	0.006
bond angles (deg)	2.1

Structural Basis for Mutagenesis and Thio Effects. There have been several published crystal structures of *h*UDG bound to duplex substrate DNA in which the glycosidic bond has been cleaved (*7*). More recently, a structure of *h*UDG in complex with duplex DNA containing a nonreactive C-glycoside analogue of deoxyuridine ("pseudouridine") was determined (*6*). However, the interesting structural question of how UDG reacts with nearly equal facility with single-stranded dU-containing DNA has not yet been addressed (*10*). Thus, we sought to obtain crystals of *e*UDG in complex with a ssDNA substrate (dUAAp) to ascertain the structural basis for the efficient recognition of both duplex and single-stranded DNA, and provide a structural basis for the interpretation of the mutational and thio effects.

The previously determined structure of free *e*UDG (*15*) and that of the new complex with dUAAp are aligned in Figure 4A, and the structural statistics for the complex are reported in Table 2. This alignment shows that binding of dUAAp brings about a clamping motion of active site loops, and movement of helix 8, that leads to optimal positioning of the active site chemical groups (vida infra). Notably, previously determined structures of *e*UDG and herpes virus UDG bound to uracil and the trinucleotide pTpTpT, respectively, did not show this conformational change, indicating that it is triggered only upon binding of dU-containing DNA (*15*, *28*). We note that dUAAp is productively bound in this complex because the glycosidic bond has been cleaved (see Figure 5B). Consequently, electron density for the uracil base but not the abasic trinucleotide is observed, possibly due to disorder in the nucleotide after bond cleavage. An alternative explanation would be that the trinucleotide has completely dissociated, which requires that the interactions with the uracil base alone result in the observed closed conformation.[4]

For comparison with the conformational change in UDG that accompanies duplex U-DNA binding, an alignment of free *h*UDG and its ternary complex with an 11mer abasic duplex DNA and uracil is shown in Figure 4B (*7*). In this

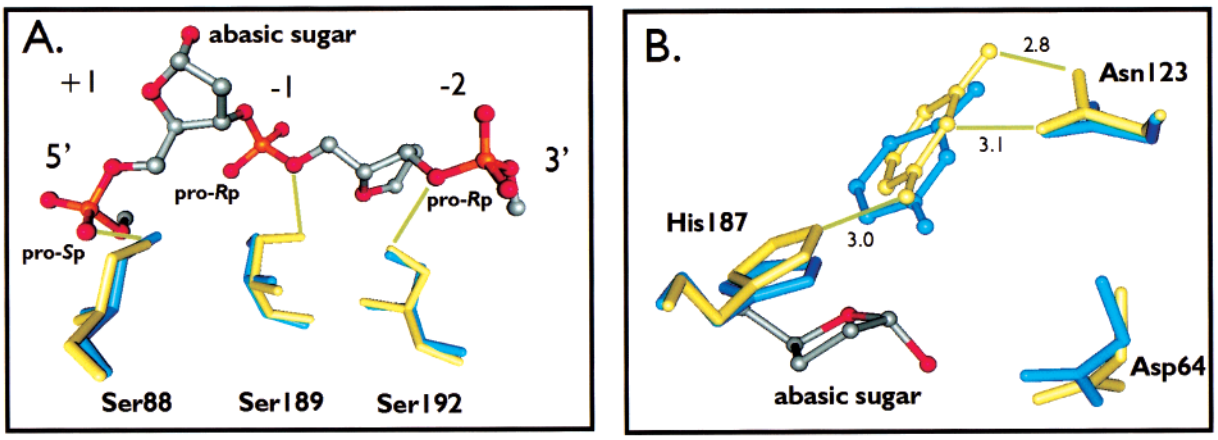

FIGURE 5: Comparison of the DNA phosphodiester and uracil interactions between the structures of the *h*UDG (blue) and *e*UDG (yellow) DNA complexes. (A) Arrangement of the serine pinch residues of *e*UDG and *h*UDG (S88, S189, and S192 of *e*UDG) as determined from the global alignment of the structures (Figure 4). A portion of the abasic DNA strand of the hUDG complex is also shown to illustrate the interactions of the serines with the phosphodiester oxygens. As determined from this alignment, the inferred hydrogen bonding interactions of the serine side chain hydroxyls of *e*UDG to the phosphodiester oxygens are indicated. These interactions are consistent with the thio effects and mutational effects. (B) Arrangement of the conserved active site residues of *e*UDG and *h*UDG that interact with the uracil base and abasic sugar. Because the abasic trinucleotide is disordered in the *e*UDG complex, the position of the abasic sugar is obtained from the hUDG complex. The most notable difference between these structures is that the plane of the uracil base is rotated by about 11°, and the O4 atom is pushed ~1 Å deeper in the uracil binding pocket of *e*UDG.

figure, the duplex DNA has been omitted for clarity, and the same clamping motion of the enzyme is seen. The identical conformations of the *e*UDG and *h*UDG DNA product complexes are more clearly seen in their aligned structures in Figure 4C (C_α rmsd = 0.9 Å). It may be concluded from this comparison that all the determinants required to trigger the conformational change are present in the trinucleotide dUAAp.

The similarities in the global conformations of the *e*UDG and *h*UDG complexes extend to the detailed interactions in the active site (Figure 5). The three serine-pinching residues are essentially superimposable when the two structures are aligned (Figure 5A), with the exception of the S189 γ-OH, which is rotated 50° from the corresponding group in the *h*UDG complex. In Figure 5A, a portion of the DNA backbone from the *h*UDG product complex is shown that includes the +1, −1, and −2 phosphodiester groups. The distances from the individual serine γ-OH groups to these phosphodiesters suggest that (i) Ser88 interacts with the +1 pro-S_p oxygen, (ii) Ser189 interacts with the 5′ bridging oxygen at the −1 position, and (iii) Ser192 interacts with the 3′ bridging oxygen at the −2 phosphodiester. These suggested interactions are consistent with the combined thio and mutational effects reported above.

The interactions with the uracil base and the conserved histidine, aspartic acid, and asparagine are also similar for the *h*UDG and *e*UDG product complexes (Figure 5B). The neutral electrophile, His187, is positioned 3.0 Å from the uracil O2 anion, to which it forms a strong hydrogen bond in solution (*10*−*12*). However, this distance is about 0.3 Å longer than the corresponding distance in the *h*UDG−duplex DNA product complex. The conserved aspartic acid, Asp64, is found to be rotated ~120° from its position in the free enzyme, and is thereby well-positioned to orient, or accept a proton, from the water nucleophile that attacks at C1′. The conserved Asn123 forms hydrogen bonds with uracil O4 and H3, although these are slightly longer than those seen in the *h*UDG complex with duplex DNA. The most notable difference between the human and bacterial complexes is that the plane of the uracil base is rotated by about 11° between the two structures, suggesting flexibility in the uracil binding pocket.

DISCUSSION

Requirements for Induced Fit. The crystal structure of the *e*UDG complex with dUAAp places an upper limit on the minimum set of substrate interactions that are needed to trigger the induced fit conformational change in UDG. Surprisingly, this minimum set does not include a 5′ phosphodiester group, which has previously been suggested to be required for catalytic activity (*21*) and DNA backbone compression (*7*). To further investigate this result, we recently examined the kinetic behavior of a similar substrate, dUAA, and found it to bind 15-fold more weakly than the optimal substrate AdUAA, and with a 500-fold reduced rate constant for the chemical step (*22*). Although these and the mutagenesis results indicate that the 5′ phosphodiester is important for binding and catalysis, the apparent binding energy derived from this group contributes only 15.4 kJ/mol ($-RT$ ln 500) toward lowering the activation barrier of this reaction. Nevertheless, the observation that the complexes of UDG with dUAAp and an 11mer dsDNA are structurally identical indicates that the enzyme can achieve its active conformation from a very localized set of substrate interactions encompassing the deoxyuridine nucleotide that need not include the 5′ phosphodiester. Thus, UDG has evolved a highly efficient mechanism for lowering the activation barrier that is largely independent of sequence effects and DNA structure.

[4] Recent NMR, tryptophan fluorescence, and Raman spectroscopy studies have forced us to conclude that uracil binding induces a closed conformation in UDG indistinguishable from that observed previously upon binding of dU-containing DNA. This is surprising in light of the crystal structures of the UDG−uracil complex, which show an open conformation that is essentially the same as the free enzyme (*15*, *28*). Thus, the current structure may represent the first crystallographic evidence for the closed form of the uracil complex.

Table 3: Analysis of Combined Effects of Mutagenesis and Thio Substitution on the Free Energy of Stabilization of the Transition State (kJ/mol)[a]

mutation	thio substitution site	interaction of nonbridging oxygen[b]	$\Delta\Delta G^{Ps+mut}$ [c]	$\Delta\Delta G^{Ps} + \Delta\Delta G^{mut}$ [d]	ΔG_c[e]	nature of coupled interaction[f]
S88A	+1 R_p	$2H_2O$	21.7	20.0	1.7	A
	+1 S_p	S88 γOH, αNH	16.7	24.9	−8.2	PC
	−1 R_p	H_2O, S189 γOH	21.0	16.9	4.1	NC
	−1 S_p	$2H_2O$	22.1	17.4	4.7	NC
S189A	+1 R_p	$2H_2O$	15.7	16.3	−0.6	A
	+1 S_p	S88 γOH, αNH	14.3	21.2	−6.9	PC
	−1 R_p	H_2O, S189 γOH	12.6	13.2	−0.6	A
	−1 S_p	$2H_2O$	13.3	13.7	−0.4	A
S192G	−2 R_p	H_2O, S166 αNH	14.6	16.1	−1.5	A
	−2 S_p	H_2O, H187 αNH	5.2	5.3	−0.1	A

[a] The free energy effects are calculated from the respective thio (Ps) effects and mutational (mut) effects on k_{cat}/K_m reported in Table 1. [b] The interaction of the nonbridging oxygen as observed in the crystal structure. [c] $\Delta\Delta G^{Ps+mut}$ is the combined effect of thio substitution and the given serine mutation, and $\Delta\Delta G^{Ps+mut} = -RT \ln[(k_{cat}/K_m)^{Ps,\,mut}/(k_{cat}/K_m)^{ox,wt}]$. The errors in $\Delta\Delta G^{Ps+mut}$ are ≤0.8 kJ/mol. [d] The sum of the individual effects of thio substitution and mutagenesis where $\Delta\Delta G^{Ps} = -RT \ln[(k_{cat}/K_m)^{Ps}/(k_{cat}/K_m)^{ox}]$ and $\Delta\Delta G^{mut} = -RT \ln[(k_{cat}/K_m)^{mut}/(k_{cat}/K_m)^{wt}]$. The errors in the sum are ≤1.5 kJ/mol. [e] The parameter ΔG_c is the coupling energy between a given nonbridging oxygen and a serine side chain, and measures the departure from additivity of the two single effects, i.e., $\Delta G_c = \Delta\Delta G^{Ps+mut} - (\Delta\Delta G^{Ps} + \Delta\Delta G^{mut})$. The errors in ΔG_c are ≤2.3 kJ/mol. [f] NC, negative cooperativity; PC, positive cooperativity; A, additive (independent). Effects are designated PC and NC only if ΔG_c is greater than the errors in the measurements.

Mapping the Energetic Coupling in Phosphodiester Pinching. In principle, the combined damaging effect of thio substitution and deleting an amino acid side chain ($\Delta\Delta G^{Ps+mut}$) can be the simple sum of the two individual effects ($\Delta\Delta G^{mut} + \Delta\Delta G^{Ps}$) or may differ from simple additivity by an amount termed the coupling energy (ΔG_c, eq 6) (*24*, *26*, *29*).

$$\Delta\Delta G^{Ps+mut} = \Delta\Delta G^{mut} + \Delta\Delta G^{Ps} + \Delta G_c \qquad (6)$$

In general, a coupling energy will be observed when either of the single alterations changes the interaction energy between the two sites. For example, if the mutation has no effect on the interaction of the nonbridging substituent, then the coupling energy will be zero, and the mutagenesis and sulfur effects will be energetically independent (i.e., $\Delta\Delta G^{Ps+mut} = \Delta\Delta G^{mut} + \Delta\Delta G^{Ps}$). On the other hand, if the mutation alters the interaction of the nonbridging substituent, for either better or worse, a positive or negative coupling energy will result, and the combined effect will deviate from simple additivity according to eq 6. The structural studies and the mutagenesis and thio effects provide a functional map of the energetic interactions between the serine pinch residues and the phosphodiester groups of the substrate as quantified in Table 3 and shown schematically in Figure 6.

Ser88. The direct interaction of Ser88 with the +1 pro-S_p oxygen is the strongest interaction observed for any of the serine pinch residues in the transition state ($\Delta G^{mut} = 14.5$ kJ/mol). As might be expected, this mutagenesis effect is similar to the effect of removing the +1 nucleotide (15.4 kJ/mol; see above). The combined analysis of the structural data, and the thio and mutational effects on k_{cat}/K_m, indicates that Ser88 forms a direct stereospecific interaction with the +1 pro-S_p oxygen ($\Delta\Delta G_c = -8.2$ kJ/mol) and is coupled indirectly to both of the −1 nonbridging oxygens ($\Delta\Delta G_c =$ 4.1 and 4.7 kJ/mol, Table 3). The strongly negative $\Delta\Delta G_c$ at the +1 S_p position reflects the 28-fold lower thio effect for S88A at this site, and would be expected on the basis of the direct interaction of this group with the +1 S_p substituent (Figure 5A). In contrast, the strongly positive $\Delta\Delta G_c$ values for the Ser88 interaction with both of the −1 positions would not be predicted by inspection of the crystal structure, or from studies of the thio effect or mutational effect alone.

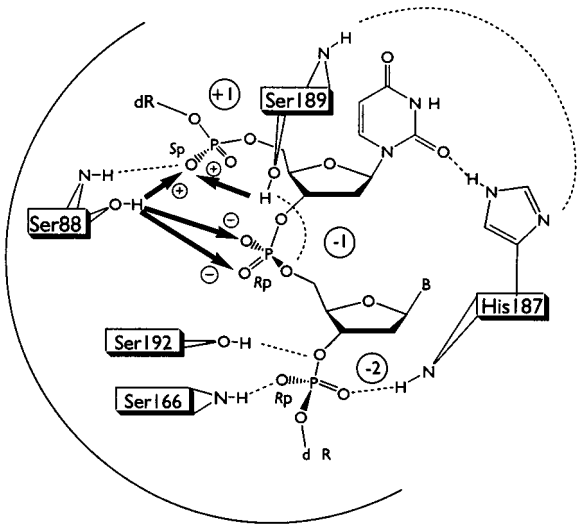

FIGURE 6: Direct and indirect coupling energies between serine pinching side chains and phosphodiester oxygens. The coupling energy may be interpreted as the additional apparent energy of interaction between the phosphodiester oxygen and the given serine residue as compared to that of the interaction with sulfur (Table 3). In this figure, bold arrows with plus and minus signs indicate cooperative and anticooperative coupling energies, respectively. Dashed lines represent hydrogen bonds. The S88A mutation causes an increased R_p and S_p thio effect at the −1 position (strain), and the S189A mutation causes a stereoselective decrease in the S_p thio effect at the +1 phosphodiester (positive cooperativity). The S189A and S192G mutations have little effect on the magnitude of the thio effects at the −1 or −2 position, indicating that these groups do not interact directly or indirectly with these nonbridging oxygens (see the text). A highly intertwined network of hydrogen bonds that connects the +1, −1, and −2 phosphodiester groups with the serine pinch residues and the electrophile His187 is indicated.

The positive coupling energy reveals the presence of strain between the Ser88 and the −1 phosphodiester (*29*). In this interpretation, when Ser88 or one of the −1 nonbridging oxygens is changed individually, not only a favorable interaction but also an unfavorable strain energy is lost. Thus, each individual change appears less damaging due to the

release of strain energy. When the effects of both changes are measured simultaneously (i.e., the reaction of the thio substrate with the mutated enzyme), two favorable interactions are lost, but strain is lost only once, leading to the result that the double effect is more damaging than the sum of the single effects. Strain may result from either electrostatic repulsion between the compressed +1 and −1 phosphodiester groups or conformational strain in the system. As noted in Table 3, this energetic coupling is an example of anticooperativity in binding the transition state.

Ser189. The combined analysis of the thio and mutational effects on k_{cat}/K_m indicates that Ser189 has a strong energetic coupling with the +1 pro-S_p oxygen, even though this group does not directly interact with the +1 position ($\Delta\Delta G_c = -6.9$ kJ/mol, Table 3 and Figure 5A). However, the absence of any significant change in the R_p and S_p thio effects at the −1 position upon removal of Ser189 indicates that this group does not interact directly or indirectly with the nonbridging oxygens of the −1 phosphodiester. This result is consistent with the crystal structure, which indicates that the Ser189 γ-OH is within hydrogen bonding distance of the 5′ bridging oxygen at the −1 position (Figure 5A). The deletion mutagenesis results indicate that the Ser189 interaction with the 5′ bridging oxygen is worth 10.8 kJ/mol toward transition-state stabilization, but only 5.5 kJ/mol toward stabilizing the ES complex, and therefore contributes about 5 kJ/mol toward lowering of the activation barrier of ES → ES‡. Taken in their entirety, these results indicate a complex pattern of energetic cross talk between 5′ and 3′ serine pinching residues and three of the four nonbridging oxygens at the +1 and −1 positions (Figure 6).

Ser192. Removal of Ser192 has an equal damaging effect on the stability of the ES complex and the transition state (∼7 kJ/mol), indicating that this group has no role in reducing the kinetic barrier of ES → ES‡. The combined analyses of the thio and mutational effects on k_{cat}/K_m indicate that Ser192 does not interact directly or indirectly with the nonbridging oxygens of the −2 phosphodiester, consistent with the crystal structure that places the Ser192 γ-OH near the 3′ bridging oxygen of the −2 phosphodiester (Figure 5A). Therefore, the large −2 R_p thio effect likely results from disruption of the favorable amide hydrogen bond from Ser166 to the pro-R_p oxygen (Figure 6). The significantly larger R_p effect as compared to the S_p thio effect at the −2 position is consistent with the shorter and presumably stronger hydrogen bond between Ser166 NH and the pro-R_p oxygen (2.75 Å), as compared to the hydrogen bond between the −2 pro-S_p oxygen and His187 NH (2.99 Å) (*7*).

An Extended and Cooperative Hydrogen Bond Network. The crystallographic and thio effect studies describe a highly interconnected network of hydrogen bonds that couple uracil flipping with phosphodiester compression and induced fit specificity. A striking example is the extended network that links the +1, −1, and −2 phosphodiester groups with Ser88, Ser189, Ser192, and the electrophile, His187 (Figure 6). Such exquisite structural preorganization in the ground state, which avoids any unfavorable reorganization energy terms in proceeding to the transition state, may account for a considerable portion of the catalytic power of UDG that cannot yet be accounted for by transition-state stabilization (*10*−*12*, *15*). Such an extended and intertwined network makes it difficult to evaluate discrete energetic contributions, because cooperative and anticooperative energetic effects between different members of the network are likely to be important (vida supra). Thus, the energetic effects that are reported above cannot entirely separate these terms, and must be considered apparent effects (*30*).

How Important Is Strain Energy in the Bond Cleavage Step? Tainer and colleagues have recently proposed a major role for ground-state strain in catalysis on the basis of the severely bent glycosidic bond in the UDG complex with deoxypseudouridine DNA (Scheme 1) (*6*).

Scheme 1

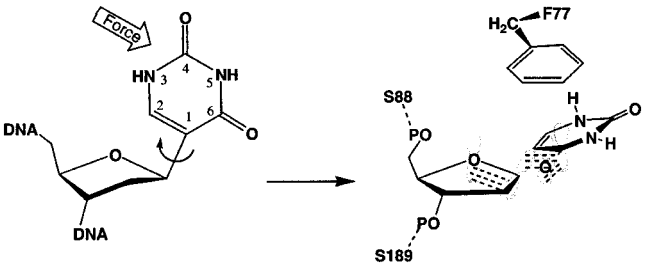

Indeed, induced strain was characterized as the missing link in understanding the catalytic power of UDG. According to this viewpoint, phosphodiester pinching flattens the sugar pucker, and assists, along with aromatic stacking forces, in bending the glycosidic bond to a remarkable tetrahedral geometry from its normally trigonal planar arrangement in deoxyuridine and deoxypseudouridine (see Figure 1 and Scheme 1). This bending is hypothesized to result in favorable overlap between the p orbital of O4′ and the conjugated π system of the uracil ring, profoundly lowering the activation barrier (Scheme 1) (*6*). It is important to point out that UDG lowers the activation barrier of the spontaneous glycosidic bond hydrolysis reaction by 68 kJ/mol at neutral pH and 25 °C, and if strain and stereoelectronic control are truly the missing energetic contributions to catalysis, a major portion of this rate enhancement must be accounted for.[5]

Since the strain mechanism seems to require secure clamping of the 3′ and 5′ phosphodiester groups, as suggested by the crystallographic studies (*6*), the damaging effect of removing these groups should provide an estimate of the possible contribution of strain and orbital steering in lowering the activation barrier. Accordingly, deletion of Ser88 or the 5′ phosphodiester leads to a 14.5 and 15.4 kJ/mol increase in the activation barrier, and removal of both Ser88 and Ser189 leads to a 22.2 kJ/mol increase (Table 1). Although these are not insignificant effects, they almost certainly overestimate the contribution of ground-state strain and orbital steering in the transition state due to the highly cooperative interactions in the active site (Figure 6). Even

[5] An alternative explanation for the apparent tetrahedral geometry at C1 of deoxypseudouridine would be that the enzyme has catalyzed tautomerization of the pseudouracil ring by removing the proton at N5 and placing it at C1. Tautomerization could be facilitated by the strong hydrogen bond from His187 to uracil O2, which has been shown by NMR to promote enolization of bound uracil (*12*). This alternative explanation for the crystallographic model is currently being investigated. The catalytic power of UDG is $\sim 10^{12}$, which may be calculated from the ratio of the enzymatic k_{max} value for the sequence AUAA (125 s^{-1}) and the rate constant for the nonenzymatic reaction at neutral pH and 25 °C ($k_{non} \sim 10^{-10}$ s^{-1}) (*31*). This rate enhancement corresponds to a 68 kJ/mol lowering of the activation barrier as compared to the uncatalyzed reaction.

if these damaging effects are entirely ascribed to strain and orbital steering contributions to catalysis, they are insufficient in magnitude to account for the majority of the catalytic power of UDG as proposed.

CONCLUSIONS

We have investigated the role of the conserved serine pinching residues of UDG in DNA binding and transition-state stabilization. Although these serine side chains do play a significant role in stabilizing the deoxyuridine nucleotide in the active site, and contribute to transition-state stabilization as well, the energetic contribution from the 3′ and 5′ serine clamps cannot account for a majority of the enormous catalytic power of UDG. Since it is difficult to envision how UDG could severely distort the glycosidic bond without assistance from these clamps, then these results suggest that either (i) glycosidic bond bending does not occur with the natural deoxyuridine substrate or (ii) reasonably efficient catalysis can occur in the absence of this conformational strain. We are currently investigating the vibrational spectra of several substrate analogues bound to UDG to further evaluate the possible role of ground-state strain in the mechanism.

REFERENCES

1. Frosina, G. (2000) *Eur. J. Biochem. 267*, 2135−2149.
2. Mosbaugh, D. W., and Bennett, S. E. (1994) *Prog. Nucleic Acid Res. Mol. Biol. 48*, 315−370.
3. Blount, B. C., Mack, M. M., Wehr, C. M., MacGregor, J. T., Hiatt, R. A., Wang, G., Wickramasinghe, S. N., Everson, R. B., and Ames, B. N. (1997) *Proc. Natl. Acad. Sci. U.S.A. 94*, 3290−3295.
4. Wei, Q., Frazier, M. L., and Levin, B. (2000) *J. Natl. Cancer Inst. 92*, 440−441.
5. Stivers, J. T., Pankiewicz, K. W., and Watanabe, K. A. (1999) *Biochemistry 38*, 952−963.
6. Parikh, S. S., Walcher, G., Jones, G. D., Slupphaug, G., Krokan, H. E., Blackburn, G. M., and Tainer, J. A. (2000) *Proc. Natl. Acad. Sci. U.S.A. 97*, 5083−5088.
7. Parikh, S. S., Mol, C. D., Slupphaug, G., Bharati, S., Krokan, H. E., and Tainer, J. A. (1998) *EMBO J. 17*, 5214−5226.
8. van Aalten, D. M., Erlanson, D. A., Verdine, G. L., and Joshua-Tor, L. (1999) *Proc. Natl. Acad. Sci. U.S.A. 96*, 11809−11814.
9. Sinnott, M. L. (1988) *Adv. Phys. Org. Chem. 24*, 113−204.
10. Drohat, A. C., Jagadeesh, J., Ferguson, E., and Stivers, J. T. (1999) *Biochemistry 38*, 11866−11875.
11. Drohat, A. C., Xiao, G., Tordova, M., Jagadeesh, J., Pankiewicz, K. W., Watanabe, K. A., Gilliland, G. L., and Stivers, J. T. (1999) *Biochemistry 38*, 11876−11886.
12. Drohat, A. C., and Stivers, J. T. (2000) *J. Am. Chem. Soc. 122*, 1840−1841.
13. Eckstein, F., and Gish, G. (1989) *Trends Biochem. Sci. 14*, 97−100.
14. Fasman, G. D. (1975) in *Handbook of Biochemistry and Molecular Biology: Nucleic Acids*, Vol. 1, CRC Press, Boca Raton, FL.
15. Xiao, G., Tordova, M., Jagadeesh, J., Drohat, A. C., Stivers, J. T., and Gilliland, G. L. (1999) *Proteins 35*, 13−24.
16. Howard, A. J., Gilliland, G. L., Finzel, B. C., Poulos, T. L., Ohlendorf, D. H., and Salemme, F. R. (1987) *J. Appl. Crystallogr. 20*, 383−387.
17. Brünger, A. T. (1992) *X-PLOR version 3.1. A System for X-ray Crystallography and NMR*, Yale University Press, New Haven, CT.
18. Sheldrick, G. M., and Schneider, T. R. (1997) *Methods Enzymol. 277*, 319−343.
19. Stivers, J. T. (1998) *Nucleic Acids Res. 26*, 3837−3844.
20. Leatherbarrow, R. J. (1998) *GraFit 4.0*, Erithacus Software Ltd., Staines, U.K.
21. Varshney, U., and van de Sande, J. H. (1991) *Biochemistry 30*, 4055−4061.
22. Jiang, Y. L., and Stivers, J. T. (2000) Unpublished results.
23. Kurpiewski, M. R., Koziolkiewicz, M., Wilk, A., Stec, W. J., and Jen-Jacobson, L. (1996) *Biochemistry 35*, 8846−8854.
24. Zhang, Y.-L., Hollfielder, F., Gordon, S. J., Chen, L., Keng, Y.-F., Wu, L., Herschlag, D., and Zhang, Z.-Y. (1999) *Biochemistry 38*, 12111−12123.
25. Hondal, R. J., Bruzik, K. S., Zhao, Z., and Tsai, M.-D. (1997) *J. Am. Chem. Soc. 119*, 5477−5478.
26. Stivers, J. T., Nawrot, B., Jagadeesh, G. J., Stec, W. J., and Shuman, S. (2000) *Biochemistry 39*, 5561−5572.
27. Frey, P. A. (1989) *Adv. Enzymol. Relat. Areas Mol. Biol. 62*, 119−201.
28. Savva, R., McAuley-Hecht, K., Brown, T., and Pearl, L. (1995) *Nature 373*, 487−493.
29. Mildvan, A. S., Weber, D. J., and Kuliopulos, A. (1992) *Arch. Biochem. Biophys. 294*, 327−340.
30. Fersht, A. R. (1988) *Biochemistry 27*, 1577−1580.
31. Shapiro, R., and Kang, S. (1969) *Biochemistry 8*, 1806−1810.

BI001532V